Journal of Manufacturing Processes 31 (2018) 240–246

Contents lists available at ScienceDirect

Journal of Manufacturing Processes

journal homepage: www.elsevier.com/locate/manpro

Effects of welding parameters on microstructures and mechanical properties of disk laser beam welded 2A14-T6 aluminum alloy joint

Lei Wang, Yanhong Wei*, Wenyong Zhao, Xiaohong Zhan, Lvbo She

College of Material Science and Technology, Nanjing University of Aeronautics and Astronautics, Nanjing 211106, China

ARTICLE INFO

Article history:
Received 26 September 2017
Received in revised form 7 November 2017
Accepted 18 November 2017

Keywords:
Disk laser beam welding
Welding parameters
2A14-T6
Microstructure
Mechanical properties

ABSTRACT

Disk laser beam welding technique is used to fabricate 2-mm 2A14-T6 aluminum alloy plates under different welding parameters. Effects of welding parameters on microstructures and mechanical properties of the weld are investigated. Grain size and porosity ratio in the disk laser welds firstly decrease, then increase with the increase of the heat input. Hardness at the fusion line and in fusion zone, tensile strength and elongation firstly increases, then decreases with the increasing heat input. When laser power is 2500 W, welding velocity is 2.0 m/min and heat input is 75 kJ/m, the finest microstructures, the minimum porosity ratio, the highest hardness and the maximum tensile strength are obtained. The fracture type in all samples is defined as a ductile fracture, and the maximum tensile strength reaches up to 261.7 MPa, about 61.2% of that of the base metal.

1. Introduction

Aluminum alloy is a promising light structural material widely used in the industry [1–3], which is usually jointed by laser beam welding (LBW) [4–7], with the advantages of fast welding speed, stable process, high energy density, high productive efficiency and small welding deformation [8,9]. However, the welding defects such as softened welded joint, weld crack, porosity defect et al. may appear during the laser welding process due to the poor weldability of aluminum alloy [10]. The developed welding process of aluminum alloy is continuously increasing to get the better welded joint. Understanding the effects of welding parameters on microstructures and mechanical properties of the weld can provide useful guidance for optimizing laser beam welding parameters of aluminum alloy.

There are many experiments carried out to investigate effects of laser welding parameters on microstructures and mechanical properties of laser beam welded aluminum alloy joints. Ancona et al. [11] investigated the effects of welding speed and laser power on the CO_2 laser beam butt welds of 3-mm AA5083 aluminum alloy. By comparing the welds obtained by operating at constant heat input, the best result was found under high laser powers and welding speeds. The hardness distributions and microstructures of the ND:YAG laser beam welded joint of Al-Li alloy were investigated by Cui et al. [12]. The research results showed that LBW caused the change of the micro-hardness, grain shape and orientations, and a disappearance of the micro-texture and precipitates. With the development of the laser technology, disk and fiber laser are gradually used in the laser beam weld of aluminum alloy. Choi et al. [13] found the disk laser weaving process could increase the fusion line length and improve the strength of the weld. In the study conducted by Zhang et al. [14], microstructures and mechanical properties of the fiber laser beam welded Al-Li alloy joint with AlSi12 filler wire were investigated. Over 80% tensile strength of the base metal in the laser beam weld was found because the formation of LiAlSi phases in the weld. Ahn et al. [15] investigated the influence of 4043 aluminum alloy filler wire on the weld quality and mechanical properties of the fiber laser welded 2024-T3 aluminum alloy joint. The addition of filler wire increased the number of finer dimples in the weld, causing the ductile fracture, as well as reduced micro hot cracks and porosities. Wang et al. [16] found the beam oscillation could improve the weld morphologies and promote the formation of equiaxed grains within the fusion zone due to stirring effect, and the beam oscillation almost had no effect on the tensile strength of the weld, but increased the ductility obviously. Besides, some works on the laser beam weld of aluminum alloy have been also conducted by Casalino et al. [17,18], Witzendorff et al. [19] and Sorgente et al. [20].

2A14 aluminum alloy is widely applied in the aerospace structures on account of its high mechanical strength, high fatigue resistance and good corrosion resistance. Some investigations on the 2A14 aluminum alloy weld have been conducted [21–23]. How-

* Corresponding author.
E-mail address: nuaadw@126.com (Y. Wei).

https://doi.org/10.1016/j.jmapro.2017.11.017
1526-6125/

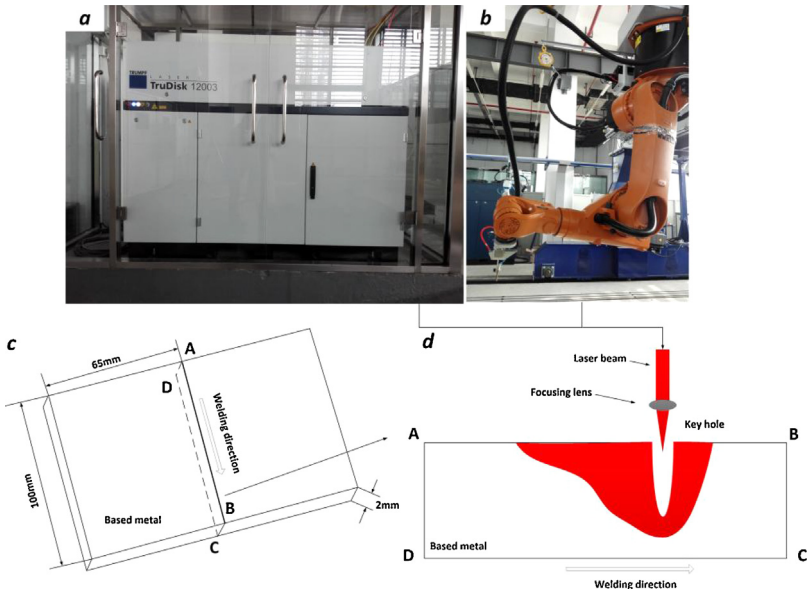

Fig. 1. Welding system including a. Laser device, b. Welding robot, c. Welding plates and d. Schematic illustration for the workpiece.

Table 1
Composition of 2A14-T6 aluminum alloy (wt%).

	Si	Cu	Mg	Zn	Mn	Ti	Ni	Fe	Al
2A14-T6	0.6~1.2	3.9~4.8	0.4~0.8	≤ 0.3	0.4~1.0	0.15	0.1	0.7	Balanced

ever, laser beam welding technique of 2A14 aluminum alloy is not investigated in detail. With the development of the disk laser technique, the disk laser beam quality, conversion efficiency and stability are greatly improved. Investigation on disk laser beam welding of 2A14 aluminum alloy is of considerable significance and desirable for optimizing welding parameters and applications. In this paper, disk laser beam welding technique is used to fabricate 2-mm 2A14-T6 aluminum alloy plates under different welding parameters. Effects of welding parameters on weld formation, grain size, porosity ratio, hardness distributions and tensile properties of the welded joint are investigated.

2. Experimental procedure

2.1. Equipment setup

Fig. 1 shows the welding system. The welding system includes a TruDisk laser device, a Kuka welding robot, and base metals. The TruDisk laser device provides the heat source for the LBW, and the Kuka welding robot attached by the laser device enables simultaneous moving. Focal length of the TruDisk laser device is 250 mm. Base metals are assembled at the focal point of the TruDisk laser device during welding. Base metals are fabricated by the butt welding, and the size of which is shown in Fig. 1c. During welding, gap between base metals is 0 mm.

2.2. Materials and welding parameters

Chemical composition of 2A14-T6 aluminum alloy is shown in Table 1. Microstructures of 2A14-T6 aluminum alloy are shown in Fig. 2. Experiments on the disk laser welding of 2-mm 2A14-T6 aluminum alloy plates are carried out. Before welding, the base metal is polished by emery papers and is cleaned using ethanol to remove the surface oxide film. Argon is used to protect the welding molten pool with the gas flow rate of 15 L/min at the top and bottom surfaces of the base metal. Based on experimental experience,

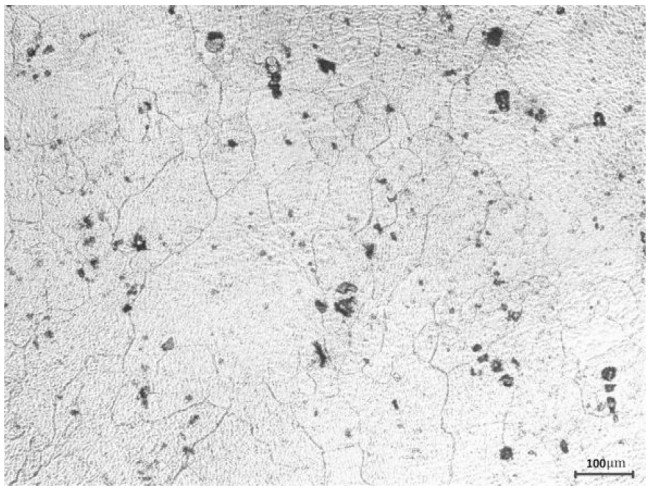

Fig. 2. Microstructures of 2A14-T6 aluminum alloy.

Table 2
Welding parameters used in welding experiments.

Case	Laser power P (W)	Welding velocity V (m/min)	Heat input H (kJ/m)
1	2500	3.0	50
2	3000	3.0	60
3	2500	2.5	60
4	3000	2.5	72
5	2500	2.0	75
6	3000	2.0	90

designed welding parameters used in welding experiments are listed in Table 2. In order to obtain accurate experimental results, each experiment is carried out three times with the average value recorded. After welding, samples are prepared by the wire cut electric discharge machine, of which cross sections are etched with

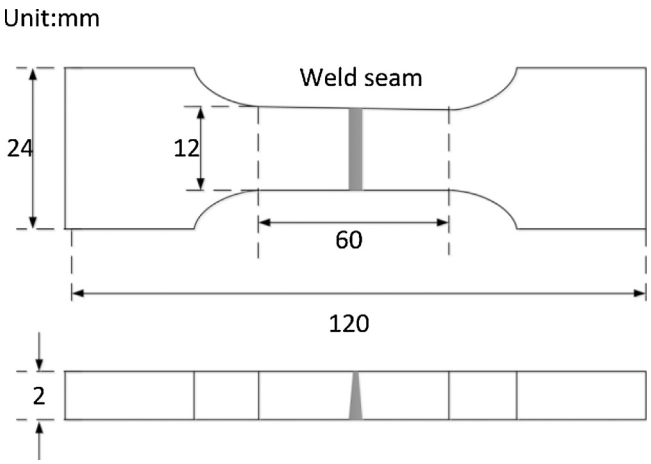

Fig. 3. Geometry of the tensile test samples.

Keller's solution (95% H_2O + 2.5% HNO_3 + 1.5% HCl + 1.0% HF) for metallographic observation. Morphologies and microstructures of the weld are observed using a MR500 metallographic microscope. Hardness of samples is measured by a HV 1000 A micro-hardness testing machine, and measurements are performed in the cross section of the weld by applying a 100 g load for 15 s. Tensile tests are performed in this study to verify the quality of the weld. Tensile samples are cut according to the China National standard [24]. A WDW-100 universal testing machine is applied to carry out the tensile test at room temperature, and the displacement speed is 1 mm/s. Fig. 3 shows the geometry of the tensile test samples. After the tensile test, the fractured surface of the weld is observed by a JSM-6360LV Scanning Electron Microscope (SEM).

3. Results and discussion

3.1. Weld formation

Fig. 4 shows the surface morphologies and cross sections of the disk laser beam welds under different welding parameters. As shown in Fig. 4e, the cross section of the weld has a typical goblet shape, and the top and bottom surfaces of the weld have the best formation under laser power of 2500 W and welding velocity of 2.0 m/min. When laser power is 2500 W and heat input is lower than 60 kJ/m, the cross section of the weld has a typical "V" shape, the top surfaces of the weld have good formation, but an incomplete fusion is found at the bottom surfaces of the weld, as illustrated in Fig. 4a and c. As shown in Fig. 4f, the fusion penetration and width are the largest, and the excess weld metal on the opposite of the weld is also the most due to the largest heat input. By comparing Fig. 4b (laser power is 3000 W, welding velocity is 3.0 m/min and heat input is 60 kJ/m) with Fig. 4c (laser power is 2500 W, welding velocity is 2.5 m/min and heat input is 60 kJ/m), it is found that higher laser power increased the fusion penetration under the same heat input. The cross sections can clearly show fusion penetration and width of the welds. The fusion penetration and width increase with the increasing heat input.

3.2. Microstructural characteristics

Microstructures of the disk laser beam welded joints of 2A14-T6 aluminum alloy under different welding parameters are shown in Fig. 5. Solidification of the welding pool starts from the fusion line to the center of the welding pool. The existing base-metal grains at the fusion boundary act as the substrate for nucleation [25]. Crystal nuclei at the fusion boundary start grow and become primary dendrites. Afterwards, the primary dendrites become coarser, and the number of that reduces due to the competitive growth. The pri-

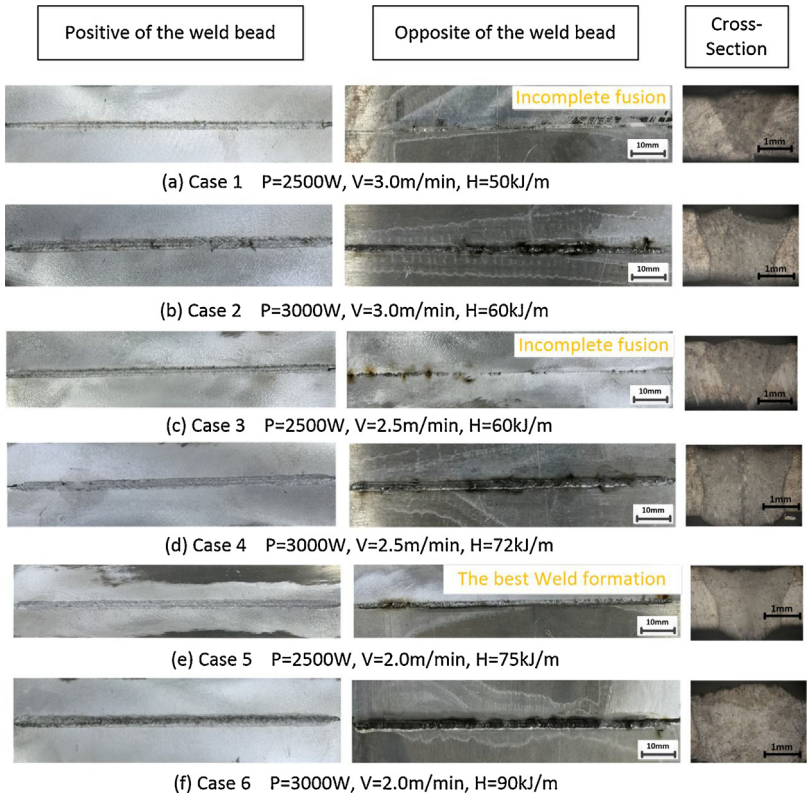

Fig. 4. Surface morphologies and cross sections of the disk laser beam welds under different welding parameters.

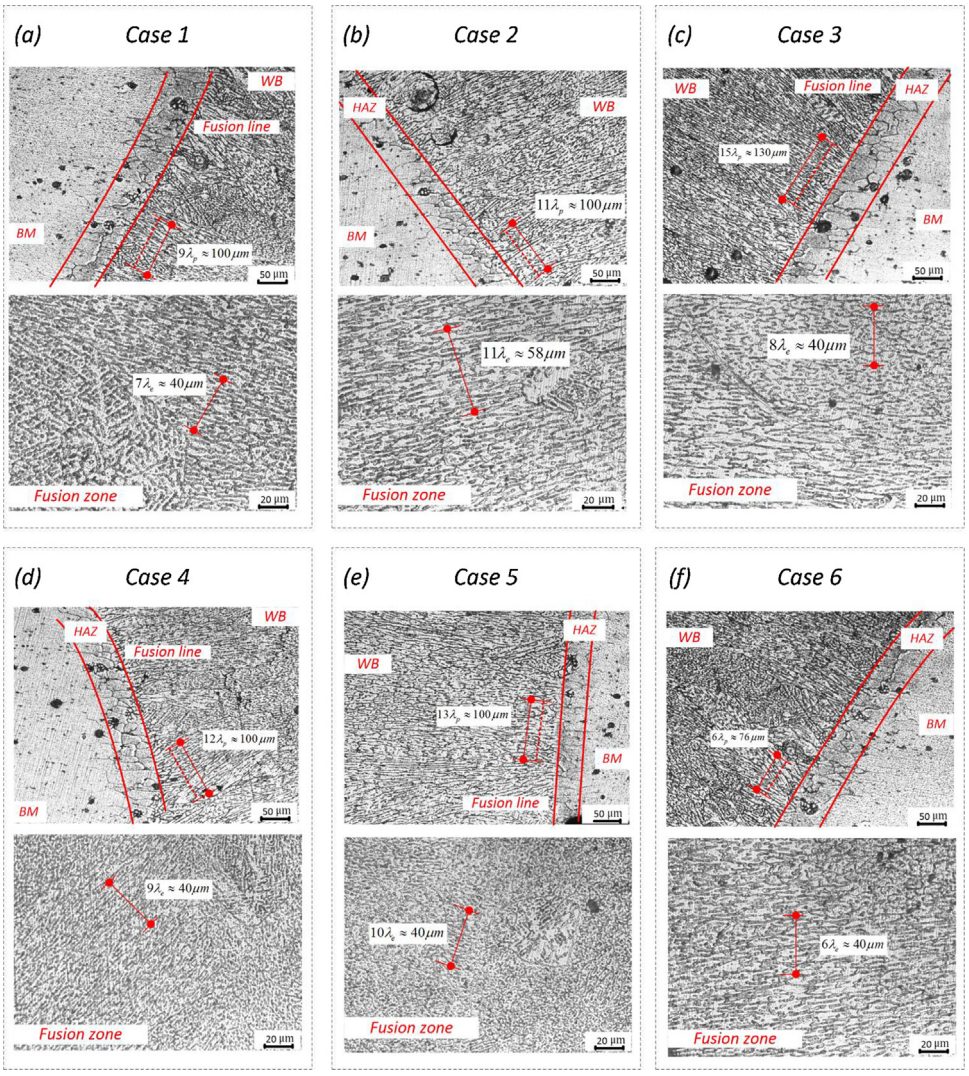

Fig. 5. Microstructures of the disk laser beam welded joints under different welding parameters.

mary dendrites grow from the fusion line to the center of the weld and along the direction of the temperature gradient. Constitutional supercooling increases in the fusion zone (FZ) with the solidification of the welding pool, and many crystal nuclei occur in FZ. Then, these crystal nuclei begin grow and become fine grains. As shown in Fig. 5, the average values of the primary dendrite arm spacing at the fusion line and grain size in FZ are measured though

$$L = n\lambda_p, L = n\lambda_e \quad (1)$$

where L is the length of the test line, n is the number of counted primary dendrites or grains, λp is the primary dendrite arm spacing at the fusion line, λe is the grain size in the fusion zone. Fig. 6 shows the evolution of the grain size with the increasing heat input in the disk laser weld. The average value of the grain size firstly decreases, then increases with the increase of the heat input. The maximum primary dendrite arm spacing (PDAS) at the fusion line and the maximum grain size in the FZ are 12.67 μm and 6.67 μm respectively when the heat input is 90 kJ/m. The minimum primary dendrite arm spacing at the fusion line and the minimum grain size in the FZ are 7.69 μm and 4.0 μm respectively when the heat input is 75 kJ/m.

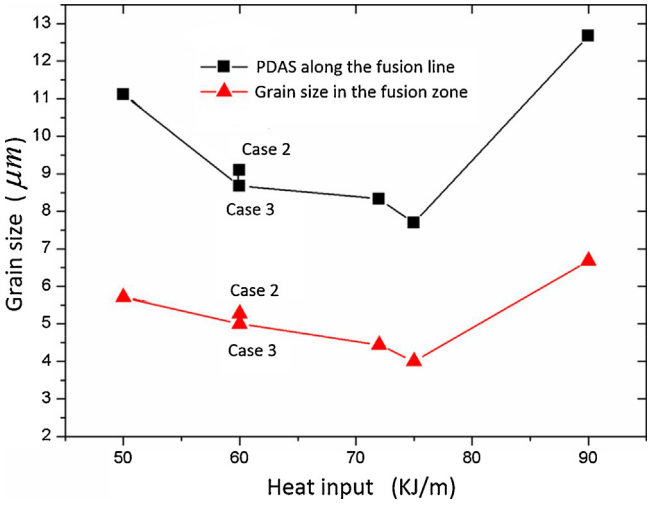

Fig. 6. Evolution of grain size with the increasing heat input in the disk laser weld under different welding parameters.

Porosity defects can be found in the welded joints. These porosity defects can strongly reduce the mechanical properties of the weld. The porosity ratio in this study is the statistical data of the proportion of porosity in the total cross-sectional area of the disk laser weld. The porosity data of the disk laser beam weld under different welding parameters is recorded in Table 3. The average

Table 3
Porosity data of the laser weld.

Case	Average area of porosity (mm^2)	Weld cross-sectional area (mm^2)	Average porosity ratio (%)	Standard deviation (%)
1	0.0128	1.12	1.14	0.062
2	0.0205	2.23	0.92	0.033
3	0.0132	1.48	0.89	0.058
4	0.0112	3.12	0.36	0.026
5	0.0055	2.76	0.20	0.018
6	0.0230	3.84	0.60	0.042

Table 4
Quantitative characterization of hardness test results.

Case	Average value in base metal (HV)	Average value in HAZ (HV)	Average value along the fusion line (HV)	Average value in the fusion zone (HV)
1	114.3	83.1	62.4	72.6
2	112.7	81.5	68.4	76.7
3	110.6	84.6	70.6	80.3
4	116.0	85.5	74.7	84.6
5	107.9	86.1	79.8	87.9
6	112.0	82.5	54.6	68.2

porosity ratio firstly decreases, then increases with the increase of the heat input. The porosity ratio of the disk laser beam weld with the heat input of 72 kJ/m and 75 kJ/m is much lower than others. These data illustrate that the porosity ratio can be effectively reduced when the heat input is control at about 75 kJ/m. When the heat input is 75 kJ/m, the porosity ratio is the lowest. When laser power is 2500 W and heat input is 50 kJ/m and 60 kJ/m, the porosity ratio is higher. The reason is that an incomplete fusion can be observed at the bottom surfaces of the weld due to the low heat input, which leads to the formation of many large porosity defects at the bottom of the weld.

3.3. Hardness distributions

Micro-hardness testing results under different welding parameters are listed in Table 4. For the same disk laser welded joint, micro-hardness is lowered at the fusion boundary, gradually increases from the heat-affected zone (HAZ) to the base metal (BM). The hardness in the center of FZ is larger than that at the fusion boundary, because gains in FZ are finer. Micro-hardness of BM is the highest, while that at the fusion boundary is the lowest. The reason of the highest micro-hardness of BM is that the BM is strengthened by solution heat treatment and ageing strengthening treatment, as the microstructures shown in Fig. 2. The reason of the lowest micro-hardness at the fusion boundary is that the strengthening effect is decreased since alloying elements are burned loss. During the welding, the welding thermal cycling makes grains coarsen and over ageing in HAZ. Therefore, micro-hardness of HAZ is lower than that of BM. As listed in Table 4, the micro-hardness in the BM and HAZ under different welding parameters is similar, while that at the fusion line and in FZ is different under different welding parameters. Micro-hardness at the fusion line and in FZ firstly increases, then decreases with the increase of the heat input. When the heat input is 75 kJ/m, the highest hardness at the fusion line and in FZ is obtained.

3.4. Tensile properties

The tensile test results are shown in Fig. 7. Fig. 8 shows the fracture surfaces of the disk laser beam welded joints under different welding parameters. All tensile fractures occurred in FZ. The tensile strength and elongation of BM are about 427.7 MPa and 10.6%, respectively. The tensile strength and elongation of the weld are much lower than that of BM due to uneven distributions of components and welding defects in the weld. As shown in Fig. 7, the tensile strength and elongation of the laser disk welded joint firstly increase, and then decrease with the increase of the heat input. When the heat input is 75 kJ/m, the maximum tensile strength of the weld is the 261.7 MPa, about 61.2% of that of BM. As shown in Fig. 8a, dimples are observed in the fracture surface of the disk laser beam weld with the heat input of 75 kJ/m, and the fracture type is defined as a ductile fracture. When laser power is 2500 W and the heat input is 50 kJ/m and 60 kJ/m, the tensile strength of the weld is the lowest because an incomplete fusion is found. The tensile strength of the weld under the heat input of 90 kJ/m is the 187.3 MPa. Fig. 8b illustrates the fracture surface of the weld. The fracture surface feature is similar to that under the heat input of 75 kJ/m. The fracture type is also a ductile fracture, and dimples are also observed in the fracture surface. The tensile strength of the weld under the heat input of 90 kJ/m is lower than that under the heat input of 75 kJ/m because porosity ratio of the former is higher than that of latter, as illustrated in Table 3. The tensile strength of the weld when the heat input is 60 kJ/m (laser power is 3000 W) and 72 kJ/m is 154.6 MPa and 167.3 MPa, respectively. As shown in Fig. 8c and d, numerous dimples are clearly seen in the fracture

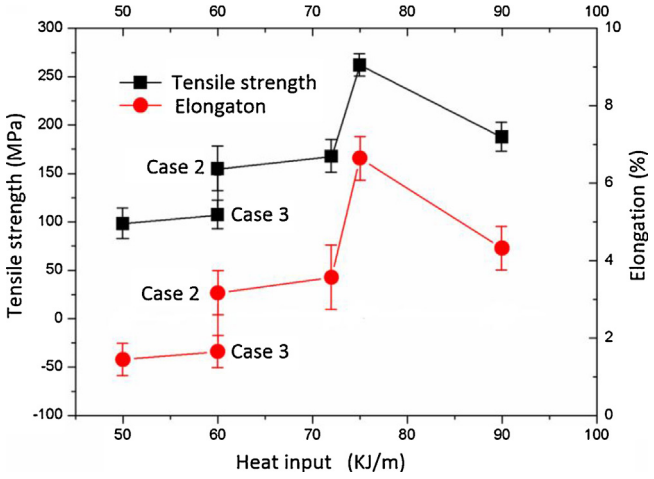

Fig. 7. Tensile strength and elongation of the laser beam weld of 2A14-T6 aluminum alloy under different heat input.

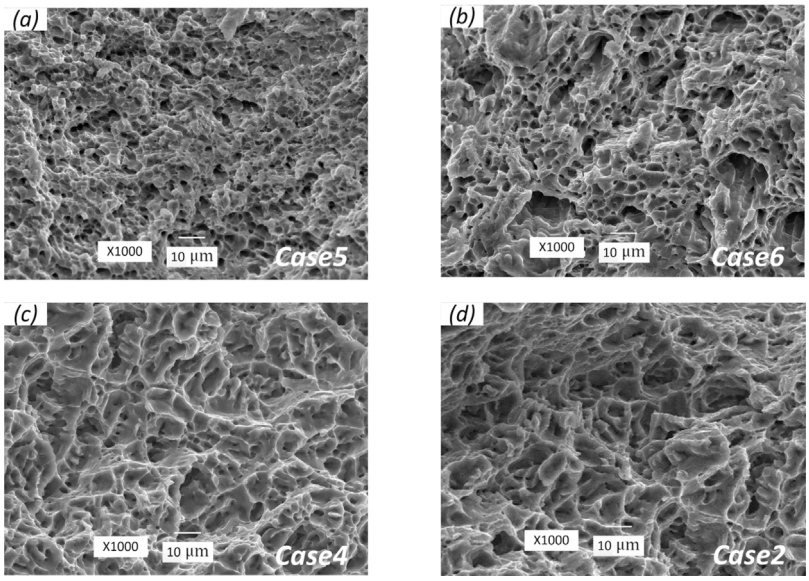

Fig. 8. Fracture surfaces of the laser beam welded joints of 2A14-T6 aluminum alloy.

surfaces of the welds. The fracture type is a typical ductile fracture. Though the average size of dimples in the case 2, case4 and case 6 is bigger than that in the case 5 as shown in Fig. 8a–d, higher porosity ratio in the case 2, case 4 and case 6 decreases the ductility of the welds. Therefore, the elongation in the case 2, case 4 and case 6 is lower than that in the case 5, as shown in Fig. 7.

4. Conclusions

Disk laser beam welding technique is used to fabricate 2-mm 2A14-T6 aluminum alloy plates under different welding parameters. Effects of welding parameters on microstructures and mechanical properties of the weld are investigated. The conclusions are as follow:

(1) When the heat input is constant, higher laser power can increase fusion penetration. Best weld formation and performances have been obtained by operating at 2500 W and 2.0 m/min.
(2) The average value of the grain size in the weld firstly decreases, then increases with the increase of the heat input. When the heat input is 75 kJ/m, the finest microstructures are obtained.
(3) Porosity ratio in the weld firstly decreases, then increases with the increasing heat input. When the heat input is 75 kJ/m, the minimum porosity ratio is obtained.
(4) Hardness in the BM and HAZ under different welding parameters is similar, while that at the fusion line and in FZ firstly increases, then decreases with the increase of the heat input. When the heat input is 75 kJ/m, the best hardness at the fusion line and in FZ is obtained
(5) Tensile strength and elongation of the laser disk welded joint firstly increase, and then decrease with the increase of the heat input. The fracture type in all samples is defined as a ductile fracture. When the heat input is 75 kJ/m, the maximum tensile strength of the weld is the 261.7 MPa, about 61.2% of that of BM.

Acknowledgements

The authors gratefully acknowledge a Project Funded by the Priority Academic Program Development of Jiangsu Higher Education Institutions (PAPD) and the financial support of the project from the Fundamental Research Funds for the Central Universities NP2016204.

References

[1] Schubert E, Klassen Zerner MI, Walz C, Sepold G. Light-weightstructures produced by laser beam joining for future applications in automobile and aerospace industry. J Mater Process Technol 2011;115:2–8.
[2] Pathak N, Bandyopadhyay K, Sarangi M, Spanda SK. Microstructure and mechanical performance of friction stir spot-welded aluminum-5754 sheets. J Mater Eng Perform 2013;22:131–44.
[3] Froes FH. Advanced metals for aerospace and automotive use. Mater Sci Eng A–Struct Mater 1994;184:119–33.
[4] Sahul M, Sahul M, Vyskoč M, Vyskoc M, Čaplovič Ľubomír, Pašák M. Disk laser weld brazing of AW5083 aluminum alloy with titanium grade 2. J Mater Eng Perform 2017;26:1–12.
[5] Sheikhi M, Ghaini FM, Assadi H. Prediction of solidification cracking in pulsed laser welding of 2024 aluminum alloy. Acta Mater 2015;82:491–502.
[6] Enz J, Kumar M, Riekehr S, Ventzke V, Huber N, Kashaev N. Mechanical properties of laser beam welded similar and dissimilar aluminum alloys. J Manuf Process 2017;29:272–80.
[7] Ojo OO, Taban E, Kaluc E. Loop travel-path of fibre laser welded alclad aa2219-O alloy. J Mater Process Technol 2017;251:118–26.
[8] Ion J. Laser beam welding of wrought aluminium alloys. Sci Technol Weld Joining 2013;5:265–76.
[9] Wang L, Wei Y, Zhan X, Yu F, Cao X, Gu G, et al. Simulation of dendrite growth in the laser welding pool of aluminum alloy 2024 under transient conditions. J Mater Process Technol 2017;246:22–9.
[10] Xiao R, Zhang X. Problems and issues in laser beam welding of aluminum–lithium alloys. J Manuf Process 2014;16:166–75.
[11] Ancona A, Lugarà P, Sorgente D, Tricarico L. Mechanical characterization of CO2 laser beam butt welds of AA5083. J Mater Process Technol 2007;191:381–4.
[12] Cui L, Li X, He D, Chen L, Gong S. Effect of ND:YAG laser welding on microstructure and hardness of an Al–Li based alloy. Mater Charact 2012;71:95–102.
[13] Choi K, Ahn Y, Kim C. Weld strength improvement for al alloy by using laser weaving method. J Laser Appl 2011;20:116–9.
[14] Zhang X, Huang T, Yang W, Xiao R, Liu Z, Li L. Microstructure and mechanical properties of laser beam-welded AA2060 Al-Li alloy. J Mater Process Technol 2016;237:301–8.
[15] Ahn J, Chen L, He E, Davies CM, Dear JP. Effect of filler metal feed rate and composition on microstructure and mechanical properties of fibre laser welded AA2024-t3. J Manuf Process 2017;25:26–36.
[16] Wang L, Gao M, Zhang C, Zeng X. Effect of beam oscillating pattern on weld characterization of laser welding of AA6061-t6 aluminum alloy. Mater Des 2016;108:707–17.
[17] Casalino G, Mortello M. Modeling and experimental analysis of fiber laser offset welding of al-ti butt joints. Int J Adv Manuf Technol 2016;83:89–98.
[18] Casalino G, Mortello M, Peyr P. Yb–yag laser offset welding of aa5754 and t40 butt joint. J Mater Process Technol 2015;223:139–49.
[19] Witzendorff PV, Hermsdorf J, Kaierle S, Suttmann O, Overmeyer L. Double pulse laser welding of 6082 aluminium alloys. Sci Technol Weld Joining 2015:42–7.

[20] Sorgente D, Corizzo O, Brandizzi M, Tricarico L. Preliminary study on the formability of a laser-welded superplastic aluminum alloy. J Mater Eng Perform 2014;23:4154–62.
[21] Zhang H, Min W, Xiao Z, Yang G. Microstructural characteristics and mechanical properties of bobbin tool friction stir welded 2A14-T6 aluminum alloy. Mater Des 2015;65:559–66.
[22] Xin Z, Yuhua C, Shanlin W. Effect of process parameters on mechanical properties of Ti/Zn/Al joint welded by friction stir welding. Rare Metal Mater Eng 2017;46:247–51.
[23] Qin HL, Zhang H, Sun DT, Zhuang QY. Corrosion behavior of the friction-stir-welded joints of 2A14-T6 aluminum alloy. Int J Miner Metall Mater 2015;22:627–38.
[24] GB/T2651-2008/ISO4136: 2001 Tensile test method on welded joints. Standardization Administration of the People's Republic of China; 2008.
[25] Kou S. Welding metallurgy. 2nd ed. Hoboken, NJ: John Wiley and Sons; 2003.